Available online at www.sciencedirect.com
ScienceDirect
International Journal of Heat and Mass Transfer 51 (2008) 210–223
International Journal of HEAT and MASS TRANSFER
www.elsevier.com/locate/ijhmt

Investigation of variable-property microchannel flows with electro-thermo-hydrodynamic interactions at constant pressure gradient or constant flow rate

P.W. Hwang, C.Y. Soong *

Department of Aerospace and Systems Engineering, Feng Chia University, Seatwen, Taichung 40724, Taiwan, ROC

Received 11 August 2006; received in revised form 5 April 2007
Available online 14 June 2007

Abstract

In the present paper, a systematic investigation on numerical modeling of variable-property microchannel flows with electro-thermo-hydrodynamic interactions is presented. General variable-property electro-thermal flow model consisting of mass, momentum, energy, electric potential and ions transport equations in dimensionless form is formulated and employed to study transport phenomena in microchannel flows. The major concerns are: (1) evaluation of the model approximations such as equilibrium ion distribution, constant-property and/or small zeta potential for non-overlap electric double layer (EDL); (2) the electro-thermo-hydrodynamic interactions under conditions of strong EDL effects, and (3) differences in microchannel flow characteristics at driving conditions of constant pressure gradient (CPG) and constant flow rate (CFR). Variations of fluid, transport and electric properties with local temperature and/or ion concentration are considered. The present results demonstrate that the variable-property model with Poisson–Boltzmann potential is an appropriate approximation for transport phenomena in microchannel flows. The results also disclose that, compared to those in CPG flows based on the same Reynolds number, effects of temperature non-uniformity and variable-property are relatively more pronounced in the CFR flows. At either CPG or CFR condition, heat transfer performance changes little with the variations of electric and flow parameters in this low Reynolds number ($Re = 0.1$) flow; while electric and flow fields can be significantly affected by variation of the governing parameters.

1. Introduction

Among the developing microtechnologies, microchannel flow is no doubt one of the significant branches for its wide applications, e.g. micro heat exchanger, lab-on-a-chip devices (pumping, mixing, thermal cycling, dispensing and separating), etc. It has been well understood that, for the hydraulic diameter or height of microchannel small enough (e.g. the order of 10 μm or less), the electrokinetic effects has become significant in the presence of electric double layer (EDL) and unbalanced ion distribution. In pressure-driven flows, the migration of the mobile ions in the liquid flow produces streaming current and streaming potential. The built potential and the conducting current, in turn, modify the pressure-driven main flow with a retarding effect. Study of the electrokinetic flows can be dated back to the earlier analyses, e.g. [1], with linearized Poisson–Boltzmann equation for solution of the electric potential. Later, Levine et al. [2] extended the analysis to the case of high zeta potential with electric potential solved with Poisson–Boltzmann equation.

In the last decade, due to the emergence of microsystem technology, microfluidics with electrokinetic effects attracts lots of attentions. A number of studies were carried out for analysis of pressure-driven electrokinetic flows in microchannels, e.g. flows between two parallel plates [3] and in rectangular ducts [4,5]. Recently, Soong and Wang [6] employed a microchannel model with one wall sliding to

* Corresponding author. Tel./fax: +886 4 24516246.
E-mail address: cysoong@fcu.edu.tw (C.Y. Soong).

0017-9310/$ - see front matter © 2007 Elsevier Ltd. All rights reserved.
doi:10.1016/j.ijheatmasstransfer.2007.04.010

Nomenclature

a	semi-height of the plate channel (m)
A_c	cross-sectional area of the channel
B	dimensionless characteristic wall-to-fluid temperature difference, $(T_1 - T_0)/T_0$
c_p	specific heat (kJ kg^{-1} K^{-1})
e	elementary charge, 1.6021×10^{-19} (C)
E	electric field vector (V m^{-1})
Ec	Eckert number, $U_0^2/c_p\Delta T_0$
E_s	streaming potential gradient (V m^{-1})
E_s^*	dimensionless streaming potential gradient, $E_s^* = ezE_sL_0/k_BT_0$
f	friction coefficient, $f = 8\tau_w/\rho U_0^2$
fRe	friction factor
G	dimensionless electric force parameter, $G = k_Bn_0T_0/\rho_0U_0^2$
H	dielectric force parameter, $H = \varepsilon_0k_B^2T_0^2/\rho_0e^2z^2L_0^2U_0^2$
h	heat transfer coefficient (W m^{-2} K^{-1})
I_c	conducting current (A)
I_i	ionic concentration gradient induced current (A)
I_s	streaming current (A)
J	Joule number, $J = (\lambda_0k_B^2T_0^2/z^2e^2)/\rho_0U_0L_0c_p\Delta T_0$
K	non-dimensional electrokinetic separation distance, $K = \kappa a$
k	thermal conductivity of liquid (W m^{-1} K^{-1})
k_B	Boltzmann constant, 1.3805×10^{-23} (J mol^{-1} K^{-1})
n_0	bulk concentration of ions (m^{-3})
Nu	Nusselt number, $2ah/k_0$
P	pressure (N m^{-2})
Re	Reynolds number, $\rho U_0a/\mu_0$
S_{ij}	strain rate, $S_{ij} = 1/2(\partial u_i/\partial x_j + \partial u_j/\partial x_i)$ (s^{-1})
T	temperature (K)
ΔT_0	characteristic wall-to-fluid temperature difference, $T_1 - T_0$ (K)
u, v	x and y-components of velocity (m s^{-1})
X, Y	dimensionless coordinates
x, y	coordinates (m)
z	valence of ions

Greek symbols

δ_T	dimensionless wall temperature difference, $(T_1 - T_2)/\Delta T_0$
ε	permittivity of liquid (C V^{-1} m^{-1})
Φ	dissipation function, $(\partial u_i/\partial x_j + \partial u_j/\partial x_i)\partial u_i/\partial x_j$ (s^{-2})
κ	Debye–Hückel parameter, $(2n_0e^2z^2/\varepsilon k_BT_0)^{1/2}$ (m^{-1})
λ	bulk electric conductivity of liquid (Ω^{-1} m^{-1})
λ_s	specific surface electric conductivity (Ω^{-1})
μ	dynamic viscosity (kg m^{-1} s^{-1})
ρ	liquid density (kg m^{-3})
ρ_e	charge density (C m^{-3})
θ	dimensionless temperature function, $\theta = (T - T_0)/\Delta T_0$
ψ	electrostatic potential (V)
ψ_s	streaming potential (V)
τ	dimensionless time, $\tau = tU_0/L_0$
τ_w	wall shear stress, $\tau_w = \mu_0(\partial u/\partial y)_w$
ζ	zeta potential (V)

Subscripts

e	exit
i	inlet
*	normalized quantity
0	reference

explore electrokinetic flows at asymmetric boundary conditions. The above studies are all theoretical analyses on the flows driven by a constant pressure gradient (CPG). Besides, to facilitate the analysis, they all restricted themselves at conditions of small zeta potential (<50 mV) and non-overlapping EDL. Numerical simulation of CPG at fully-developed flow condition was performed [7]. For a study of combined pressure gradient and electroosmotic pumping liquid flow in microchannels [8–10]. Among these, fluid properties at isothermal conditions were used in [8,9], whereas in [10], besides the Joule heating, only the electric conductivity and fluid viscosity were assumed temperature-dependent. By using Nernst–Planck equation for solution of the ion distributions, Chen et al. [11] analyzed numerical solutions of developing flow driven at a condition of constant flow rate (CFR) in a parallel slit microchannel. In summary of the above review, only the last analysis [11] accounted for ion concentration-dependence of electric conductivity, while the others considered constant properties.

Although the CPG flow is a common model employed in the previous studies of microchannel flows, driving condition of CFR is significant in some practical applications, where a precision flow-rate control is extremely important such as the drug delivery systems. Similar as well as dissimilar natures of the electrokinetic flows driven at CPG and CFR conditions are significant for better understanding of the fundamental microfluidic characteristics. For the flow with a non-uniform temperature field, the physical (fluid, transport, and electric) properties may vary with the local fluid temperature. In a recent work on rotating electrokinetic flow [12], the influences of the temperature-dependence of the physical properties were demonstrated. Through the coupling natures of electric, thermal, and flow fields, this class of microfluidics can be influenced by the electro-thermal hydrodynamic interactions.

Three major concerns of the present numerical study are (1) formulation of general variable-property electro-thermal flow model and evaluation of its various approximations, (2) effects of governing parameters on the electro-thermo-hydrodynamic interactions under the conditions of strong EDL effects, and (3) differences in microchannel flow characteristics at driving conditions of CPG and CFR. A general model and its approximations of various levels in dimensionless form are formulated. Comparing the predictions using different models, the effects of variable properties on the field solutions and the appropriateness of the approximate models are explored. In the present study, the numerical computations of CPG flows at lower ζ-potentials are compared with the previous analytic solutions for validation and, then, the electro-thermo-hydrodynamic characteristics at CPG and CFR conditions with higher ζ-potentials and non-isothermal effects are presented. Volumetric flow rate in CPG flow and pressure drop generated in CFR flow are also evaluated.

Although the model formulated enables a three-dimensional analysis, we adopt two-dimensional (2-D) microchannel flow as the model configuration in the present study. The reasons are 2-fold and addressed as follows. Firstly, in most practical cases, microchannels are significantly wider than depth as a consequence of the micromachining technique [13]. In a review paper of micromixers [14], it was reported that the available mixing channels are of height-to-width ratios in a wild range. The 2-D configuration can be an approximation for microchannels of small height-to-width aspect ratios used in practical applications. Secondly, except the flows with strong three-dimensional effects, the 2-D analysis may provide useful information to explore physical mechanisms of the complicated electro-thermal flows.

2. Modeling of electro-thermal flows at microscales

2.1. General model in vector form

In general, liquid is assumed incompressible and thus the compression work can be neglected. Considering the influences of local temperature and ion concentration on fluid properties, the vector form of variable-property electro-thermal flow equations, i.e., continuity, momentum conservation, thermal energy conservation, ion transport (Nernst–Planck) and electrical potential (Poisson) equations, are depicted as follows:

$$\nabla \cdot \mathbf{V} = 0, \tag{1}$$

$$\rho \partial \mathbf{V}/\partial t + \rho \mathbf{V} \cdot \nabla \mathbf{V} = \nabla \cdot (2\mu S_{ij}) - \nabla P + \rho_e \mathbf{E} - (1/2)\mathbf{E}^2 \nabla \varepsilon, \tag{2}$$

$$\rho \partial (c_p T)/\partial t + \rho \mathbf{V} \cdot \nabla (c_p T) = \nabla \cdot (k \nabla T) + \mu \Phi + \lambda \mathbf{E}^2, \tag{3}$$

$$\partial n_i/\partial t + (\mathbf{V} \cdot \nabla) n_i = \nabla \cdot (D_i \nabla n_i) + \nabla \cdot [(e n_i z_i D_i / k_B T) \nabla \psi], \tag{4}$$

$$\nabla \cdot (\varepsilon \nabla \psi) = -\rho_e = -\sum_i e n_i z_i, \tag{5}$$

where $\mathbf{V}$ is the velocity vector, P the pressure, T the temperature, Φ the dissipation function, n_i the ith ion concentration, ψ the electric potential, t the time variable, and k_B the Boltzmann constant. The fluid/transport properties, including the viscosity μ, the thermal conductivity k, the specific heat c_p, the permittivity ε, the ion diffusivity D_i, and the bulk liquid electric conductivity λ, are considered to be variable. The electric charge density is evaluated by $\rho_e = \sum_i e n_i z_i$ with the elementary charge e, and the concentration n_i and valance z_i of the ith ion. The last two terms in Eq. (2) are related to the electric forces, of which the first term stands for the Coulomb force and the second term for the dielectric force. The electric field $\mathbf{E}$ can be expressed as $\mathbf{E} = -\nabla\psi - \mathbf{E}_e + \mathbf{E}_s$, where ψ stands for the electrostatic potential distribution, $\mathbf{E}_e$ for the externally applied electric field, and $\mathbf{E}_s = \boldsymbol{\psi}_s/L$ for the streaming potential gradient induced in a forced flow, where $\boldsymbol{\psi}_s$ is the streaming potential and L is the channel length. In a straight channel streaming potential has only one component ψ_s along the channel. At steady state, the streaming potential along the flow channel can be evaluated by balancing the currents in the flow field, i.e., $I_i + I_c + I_s = 0$, where the current due to ion distribution I_i, the streaming current I_s, and the conducting current I_c are, respectively,

$$I_i = \int_{A_c} e\left(D_+ z_+ \frac{\partial n_+}{\partial x} + D_- z_- \frac{\partial n_-}{\partial x}\right) \mathrm{d}A_c = \int_{A_c} ez\left(D_+ \frac{\partial n_+}{\partial x} - D_- \frac{\partial n_-}{\partial x}\right) \mathrm{d}A_c, \tag{6}$$

$$I_s = \int_{A_c} u \rho_e \, \mathrm{d}A_c, \tag{7}$$

$$I_c = E_s \int_{A_c} \lambda \, \mathrm{d}A_c + 2wE_s\lambda_s, \tag{8}$$

in which A_c and w, respectively, denote cross-sectional area and width of the channel. It is supposed that the effect of surface conductivity λ_s is relatively small and not considered in the present analysis, $I_c \approx E_s \int_{A_c} \lambda \, \mathrm{d}A_c$, therefore, one has streaming potential gradient cross the microchannel length,

$$E_s = -\frac{\int_{A_c} \left[u\rho_e - ez\left(D_+ \frac{\partial n_+}{\partial x} - D_- \frac{\partial n_-}{\partial x}\right)\right] \mathrm{d}A_c}{\int_{A_c} \lambda \, \mathrm{d}A_c} \tag{9}$$

In energy equation (3), the Joule heating rate $\lambda \mathbf{E}^2$ and viscous dissipation rate $\mu\Phi$ are two terms of heat generation. As a strong electric field is applied, the Joule heating may become important in the thermal energy balance.

2.2. Variable-property flow model in dimensionless form

The above governing equations can be transformed into a dimensionless form. Since the extension of the non-dimensionalization procedure of two-dimensional flow equations to three-dimensional ones is trivial, without loss of generality, development of governing equation (1) to (5) for two-dimensional microchannel flows is performed. Consider the microchannel of length L and height $2a$ in

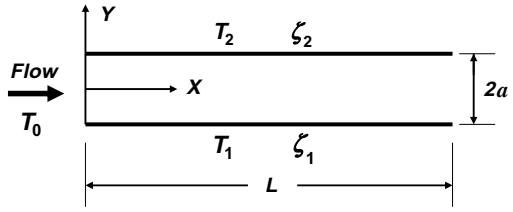

Fig. 1. Physical model of the two-dimensional microchannel flow driven at constant pressure gradient (CPG) or constant flow rate (CFR).

Fig. 1 with the following normalized variables and dimensionless parameters

$$u^* = u/U_0, \quad v^* = v/U_0, \quad X = x/L_0, \quad Y = y/L_0,$$

$$P^* = P/(\rho_0 U_0^2), \quad \psi^* = ez\psi/k_B T_0,$$

$$\zeta^* = ez\zeta/k_B T_0,$$

$$E^* = ezEL_0/k_B T_0, \quad \tau = tU_0/L_0, \quad \rho_e^* = \rho_e/(ezn_0),$$

$$\theta = (T - T_0)/\Delta T_0,$$

$$n_\pm^* = n_\pm/n_0, \quad \varepsilon^* = \varepsilon/\varepsilon_0, \quad \mu^* = \mu/\mu_0,$$

$$k^* = k/k_0, \quad c_p^* = c_p/c_{p0}, \quad \lambda^* = \lambda/\lambda_0,$$

$$K = L_0\kappa = L_0\sqrt{2n_0 e^2 z^2/\varepsilon_0 k_B T_0},$$

$$Re = \rho_0 U_0 L_0/\mu_0, \quad G = k_B n_0 T_0/\rho_0 U_0^2,$$

$$H = \varepsilon_0 k_B^2 T_0^2/\rho_0 e^2 z^2 L_0^2 U_0^2,$$

$$Sc_\pm = \mu_0/\rho_0 D_{\pm 0}, \quad Pr = c_{p0}\mu_0/k_0, \quad E_c = U_0^2/c_p \Delta T_0,$$

$$J = (\lambda_0 k_B^2 T_0^2/z^2 e^2)/\rho_0 U_0 L_0 c_p \Delta T_0$$

In the above expressions, the notations with the subscript 0 denote characteristic (reference) quantities, Re is the Reynolds number, G the electric force parameter, H the dielectric force parameter, $Sc_\pm$ the Schmidt number, Pr the Prandtl number, Ec the Eckert number, and J the Joule number. The parameter $K = L_0\kappa$ is a dimensionless parameter named the electrokinetic separation distance, whereas $\kappa = (2n_0 e^2 z^2/\varepsilon_0 k_B T_0)^{1/2}$ is the so-called Debye–Hückel parameter, and its inversion, κ^{-1}, is referred to as the characteristic thickness of EDL. The characteristic length L_0 is semi-height of the channel, i.e., $L_0 = a$. For $z - z$ symmetric electrolyte, $z_+ = -z_- = z$, the resultant dimensionless equations in conservative form are

$$\frac{\partial u^*}{\partial X} + \frac{\partial v^*}{\partial Y} = 0 \tag{10}$$

$$\frac{\partial u^*}{\partial \tau} + \frac{\partial}{\partial X}\left(u^* u^* - \frac{2}{Re}\mu^* \frac{\partial u^*}{\partial X}\right) + \frac{\partial}{\partial Y}\left(v^* u^* - \frac{1}{Re}\mu^* \frac{\partial u^*}{\partial Y} + \frac{\partial v^*}{\partial X}\right) = -\frac{\partial P^*}{\partial X} + G\rho_e^* E_x^* - \frac{1}{2}HE^{*2}\frac{\partial \varepsilon^*}{\partial X} \tag{11}$$

$$\frac{\partial v^*}{\partial \tau} + \frac{\partial}{\partial X}\left(v^* u^* - \frac{1}{Re}\mu^* \frac{\partial v^*}{\partial X} + \frac{\partial u^*}{\partial Y}\right) + \frac{\partial}{\partial Y}\left(v^* v^* - \frac{2}{Re}\mu^* \frac{\partial v^*}{\partial Y}\right) = -\frac{\partial P^*}{\partial Y} + G\rho_e^* E_y^* - \frac{1}{2}HE^{*2}\frac{\partial \varepsilon^*}{\partial Y} \tag{12}$$

$$\frac{\partial c_p^* \theta}{\partial \tau} + \frac{\partial}{\partial X}\left(c_p^* u^* \theta - \frac{1}{RePr}k^* \frac{\partial \theta}{\partial X}\right) + \frac{\partial}{\partial Y}\left(c_p^* v^* \theta - \frac{1}{RePr}k^* \frac{\partial \theta}{\partial Y}\right) = \frac{Ec}{Re}\mu^* \Phi^* + J\lambda^* E^{*2} \tag{13}$$

$$\frac{\partial n_\pm^*}{\partial \tau} + \frac{\partial}{\partial X}\left[u^* n_\pm^* - \frac{1}{ReSc_\pm}D_\pm^* \frac{\partial n_\pm^*}{\partial X} \mp \frac{1}{ReSc_\pm}D_\pm^* \frac{n_\pm^*}{(1 + B\theta)}\frac{\partial \psi^*}{\partial X}\right] + \frac{\partial}{\partial Y}\left[v^* n_\pm^* - \frac{1}{ReSc_\pm}D_\pm^* \frac{\partial n_\pm^*}{\partial Y} \mp \frac{1}{ReSc_\pm}D_\pm^* \frac{n_\pm^*}{(1 + B\theta)}\frac{\partial \psi^*}{\partial Y}\right] = 0 \tag{14}$$

$$\frac{\partial}{\partial X}\left(\varepsilon^* \frac{\partial \psi^*}{\partial X}\right) + \frac{\partial}{\partial Y}\left(\varepsilon^* \frac{\partial \psi_*}{\partial Y}\right) = K^2 \frac{n_-^* - n_+^*}{2} \tag{15}$$

In the present flow configuration, the streaming potential appears in x-direction only. Without electric field applied externally, the components of the electric field are $E_x^* = E_s^*$ and $E_y^* = 0$. To complete the model, the dimensionless form of the streaming potential gradient, $E_s^* = ezE_s L_0/k_B T_0$, is needed, *viz.*

$$E_s^* = -\frac{e^2 z^2 n_0 U_0 L_0}{k_B T_0 \lambda_0}\left[\frac{\int_{A_c^*} u^* \rho_e^* \, dA_c^*}{\int_{A_c^*} \lambda^* \, dA_c^*} + \frac{D_{+0}}{U_0 L_0}\cdot\frac{\int_{A_c^*} D_+^* \frac{\partial n_+^*}{\partial x} \, dA_c^*}{\int_{A_c^*} \lambda^* \, dA_c^*} - \frac{D_{-0}}{U_0 L_0}\cdot\frac{\int_{A_c^*} D_-^* \frac{\partial n_\pm^*}{\partial x} \, dA_c^*}{\int_{A_c^*} \lambda^* \, dA_c^*}\right] \tag{16}$$

For the boundary condition of isothermal walls, the related thermal parameters are the characteristic wall-to-fluid temperature difference, $\Delta T_0 \equiv T_1 - T_0$ and the wall-temperature difference, $\delta_T = (T_1 - T_2)/\Delta T_0$ with $B = \Delta T_0/T_0$ and $T_0 = 298$ K.

2.3. Approximations of various levels

For the above general model, the approximations used in the conventional thermal-fluid analyses such as constant-property and fully-developed conditions can be employed to simplify the problem as necessary. Besides, approximations in solution of the electric potential are most noteworthy. The electric potential can be obtained by solving the Poisson equation, Eq. (15), with the ion concentrations from Nernst–Planck equations, Eq. (14), in which general considerations of ion convection, level of zeta potential, EDL overlap, variable properties and non-isothermal effects are encompassed. This is the Poisson–Nernst–Planck (PNP) model for solution of the electric potential.

At equilibrium state, the ion concentrations can be described by Boltzmann distribution, i.e. $n_\pm = n_0 \exp(\mp ez\psi/k_B T)$, and there is no need to solve Nernst–Planck

equations. The charge density can be expressed as $\rho_e = ez(n_+ - n_-) = -2n_0 ez\sinh(ez\psi/k_B T)$. Then, Eq. (15) can be written in the form of the so-called Poisson–Boltzmann (PB) equation, viz.

$$\frac{\partial}{\partial X}\left(\varepsilon^*\frac{\partial\psi^*}{\partial X}\right)+\frac{\partial}{\partial Y}\left(\varepsilon^*\frac{\partial\psi^*}{\partial Y}\right)=K^2\sinh\left(\frac{\psi^*}{1+B\theta}\right) \tag{17}$$

To simplify the problem and facilitate the analysis, approximations such as neglecting the ion convection and assuming the ion distributions to be at equilibrium state with EDL either no or low-degree overlapping are usually employed. As the Debye–Hückel approximation for small zeta potential, $\sinh[\psi^*/(1+B\theta)] \approx \psi^*/(1+B\theta)$, is invoked, Eq. (17) can be further simplified to the linearized Poisson–Boltzmann (LPB) equation

$$\frac{\partial}{\partial X}\left(\varepsilon^*\frac{\partial\psi^*}{\partial X}\right)+\frac{\partial}{\partial Y}\left(\varepsilon^*\frac{\partial\psi^*}{\partial Y}\right)=\frac{K^2\psi^*}{1+B\theta}. \tag{18}$$

Without solving the additional nonlinear partial differential equations for ion distributions ($n_\pm$), the simplified models, PB and LPB, need relatively less computational efforts than the nonlinear PB model but their applications are restricted by the assumptions invoked.

2.4. Boundary conditions and initial guesses

The inlet conditions are $u^* = 1$, $v^* = 0$, $\psi^* = 0$, and $\theta = 0$. At walls, the conditions for velocity $u^* = v^* = 0$ the potential $\psi^* = \zeta_1^*$ and $\psi^* = \zeta_2^*$, and the temperatures $\theta = \theta_1$ and $\theta = \theta_2$ are imposed. Since this class of extremely low Reynolds number flows becomes fully developed in a very short entry length, the conditions $\partial u^*/\partial X = \partial v^*/\partial X = \partial\psi^*/\partial X = \partial\theta/\partial X = 0$ are employed at the downstream boundary of the computational domain for CFR flow. While for CPG flows, the flow rate or mean velocity is not known a priori, periodic boundary conditions are posed at inlet and exit of the channel. The initial guesses for all variables are set to be zero, while the reference value is used for temperature field to initiate the computation.

2.5. Numerical method

The governing equations are discretized by finite volume method and solved on non-uniform grid systems. All variables are stored and computed at control volume center, and the values at the center of control surface are obtained by linear interpolation that is a second-order approximation on both uniform and non-uniform grids [15]. For convection terms in the equations, to overcome the drawback of non-diagonal dominance of the coefficient matrices stemmed from central differencing, the deferred correction procedure blending upwind and central-difference schemes is employed. The pressure-velocity coupling is treated with SIMPLEC algorithm [16], which is one of the SIMPLE-based solution methods [17–20]. The pressure interpolation at cell faces is employed to avoid unrealistic pressure oscillations. The system of discretized algebraic equations is solved by SIP method [21].

3. Results and discussion

3.1. Description of governing parameters

Consider microchannel flow configuration shown in Fig. 1 with 1–1 infinite dilute electrolyte KCl of concentration $n_0 = 10^{-6}$ M, the characteristic length a of order 1 μm or 10 μm, and the zeta potential $0 \leqslant \zeta \leqslant 200$ mV. The reference velocity U_0 is the mean velocity U_m in the channel. For flows at CFR condition, U_m can be evaluated from the given flow rate and the value corresponding to the baseline one at $Re = 0.1$ is employed; while for CPG, pressure gradient across the channel length L, $\Delta P/L$, is prescribed rather than the flow rate or the mean velocity. In definition of Re, therefore, the mean velocity corresponding to the baseline case of Poseuille flow with a given pressure gradient, i.e., $U_m = -a^2(\Delta P/L)/3\mu$, is used. With the appropriate values of pressure gradient or flow rate, in the present study, the corresponding dimensionless zeta potential $0 \leqslant \zeta^* \leqslant 8$, the electrokinetic separation distance K between 0.5 and 50, and the Reynolds numbers $Re = 0.1$ are used through the present computational work. The inlet fluid temperature is $T_0 = 298$ K. The thermal parameters $B \equiv \Delta T_0/T_0 = (T_1 - T_0)/T_0$ and $\delta_T = (T_1 - T_2)/\Delta T_0$, in the non-isothermal computational cases are evaluated with $T_2 = T_0 = 298$ K and $\Delta T_0 = 0$–60 K, thus, $\delta_T = 1$, $B = 0$–0.2. Based on the above parameters with typical values of $K \sim 10$ and $\Delta T_0 \sim 10$ K, the Coulomb force parameter G is $O(1)$; while the other dimensionless parameters, H for dielectric force is $O(10^{-2})$, Ec for viscous dissipation is $O(10^{-8})$, and J for Joule heating is $O(10^{-9})$. Although the latter three has minor influences on the present flow configuration, we still retain their effects in the models for completeness of the numerical models but will not present detailed parametric study on these effects.

Since the liquid flow under consideration is a very dilute solution, the fluid properties of water are used in the simulations. The viscosity μ, the thermal conductivity k, the permittivity ε, the ion diffusivity D_i, and the bulk liquid electric conductivity λ are considered as variable and the correlations of the dimensionless parameters $\mu^*(\theta), k^*(\theta), \varepsilon^*(\theta)$, $\lambda^*(n_\pm^*, \theta)$, and $D_\pm^*(\theta)$ are presented in Appendix A. Additionally, the variation of the specific heat c_p is assumed constant or $c_p^*(\theta) = 1$ for its relatively small variation with fluid temperature in the ranges of parameters considered in the present work.

3.2. Grid test and code validation

Non-uniform grid clustered towards walls is arranged for the presence of high potential gradients at high-K condition. In all cases studied, the smallest grid size of $10^{-5}a$

Table 1
Grid-dependence of PB-V predictions of E_s^*, $(\partial\psi^*/\partial Y)_1$, and $(\partial\psi^*/\partial Y)_2$ for a CPG flow at $Re = 0.1, K = 50, \zeta_1^* = 8, r_\zeta = 1, B = 0.2, \delta_T = 1$

Grid no.	E_s^*	Error* (%)	$(\partial\psi^*/\partial Y)_1$	Error (%)	$(\partial\psi^*/\partial Y)_2$	Error (%)
502 × 27	0.177879	1.733	−1687.837987	−3.790	2608.027486	−4.312
502 × 52	0.175739	0.510	−1734.199781	−1.143	2693.984044	−1.159
502 × 77	0.175179	0.190	−1746.787187	−0.426	2713.704411	−0.435
502 × 102	0.174996	0.085	−1750.917575	−0.191	2720.223577	−0.196
502 × 127	0.174915	0.039	−1752.74224	−0.086	2723.125051	−0.089
502 × 152	0.174873	0.014	−1753.698819	−0.032	2724.657493	−0.033
502 × 177	0.174848	0	−1754.259618	0	2725.562552	0

* Errors are evaluated with the results on the finest grid of 502 × 177 as reference.

next to walls is employed. For the present flow at the low Reynolds number $Re = 0.1$, the numerical solutions demonstrate that the flow is fully developed at very short entrance length, say $X < 1$. However, considering the appropriateness of imposing fully-developed conditions and economics in computational time, the microchannel of length $40a$ is used. Simulations using variable-property model for the flows at $Re = 0.1$ with parameters $K = 50$, $\zeta^* = 8$, $r_\zeta = 1$, $B = 0.2$, and $\delta_T = 1$ are carried out to examine the grid-dependence of the predictions. Since the solutions are not sensitive to the variations in x-direction, the grid number in x-direction (502) is fixed in the grid-independence test, while that in y-direction is changed from 27 to 177, i.e. 502 × 27, 502 × 52, 502 × 77, 502 × 102, 502 × 127, 502 × 152, and 502 × 177. The predictions of the streaming potential gradient, E_s^*, and the potential gradient at walls, $(\partial\psi^*/\partial Y)_1$ and $(\partial\psi^*/\partial Y)_2$, are shown in Table 1. It is evident from the data listed that the deviation of the solutions obtained on the grid systems of 502 × 152 and 502 × 177 are within 0.035%. This concludes the grid-independence and the grid of 502 × 152 is employed through this study.

To verify the present numerical predictions, isothermal flows driven at CPG with various electrokinetic conditions are examined. Since the streaming potential gradient E_s^* is a consequence of electro-hydrodynamic interaction, E_s^* in some typical cases predicted using various models are shown in Fig. 2a for comparison. In Fig. 2a, the predictions at $Re = 0.1, \zeta_1^* = 4, r_\zeta = 1, \delta_T = 1, B = 0, 0.1$ and $K = 3$, 10, 50 are presented. It is observed that the numerical results using LPB model with constant properties agree almost exactly with the analytic solutions [6].

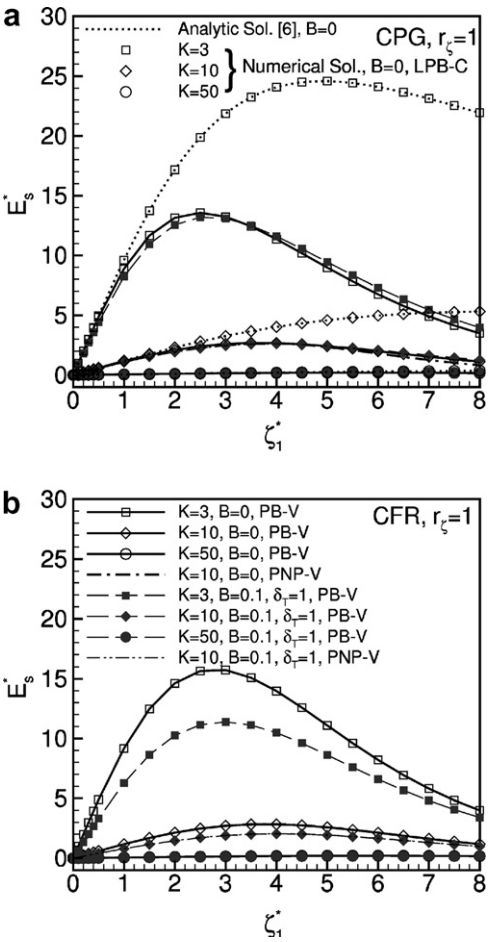

Fig. 2. Comparisons of various models for streaming potential gradients in microchannel flows driven at a (a) constant pressure-gradient; and (b) constant flow rate.

In previous analytic/numerical investigations, reduced models with constant properties were usually used. To systematically compare the performance of these models, in the following presentation the computational results predicted using the electric potential models of PNP, PB, and LPB are examined. For each of the above three models, the following three situations of the fluid and transport properties are considered: (1) μ, k, ε, λ, $D_\pm$ = constant – constant-property flow; (2) μ, k, ε = constant, and λ, $D_\pm = f(n_\pm)$ – the fluid viscosity, thermal conductivity, and permittivity are constant but the electrical conductivity and ion diffusivities are functions of ion concentration; and (3) μ, k, $\varepsilon = f(T)$, and λ, $D_\pm = f(n_\pm, T)$ – the fluid viscosity, thermal conductivity, and permittivity are functions of local fluid temperature, and the electrical conductivity and ion diffusivities are functions of both local ion concentration and fluid temperature. For brevity, C, IC, and V, respectively, are used to denote the above three situations, i.e., (1) constant-property (C); (2) properties varying with ion concentration (IC), and (3) all properties variable (V). For example, PB-V stands for the flow model with variable properties and the electric potential solution by Poisson–Boltzmann equation.

3.3. Comparisons of various models with/without influences of local temperature and ion distributions

To explore the deviations in predictions using approximate models, the numerical solutions of E_s^* with various models are compared. In Fig. 2, the results with $B = 0$ are constant-property flow solutions, and the data at $B = 0.1$ and $\delta_T = 1$ are non-isothermal solutions generated by variable-property flow models. Relatively, the linearization of PB equation causes major deviation, and the deviation becomes more remarkable with increasing EDL effects at a larger zeta potential (ζ_1^*) and/or a smaller Debye–Hückel parameter (K). Whereas predictions with PB and PNP solutions of electric potential agree fairly well for both CPG and CFR flows in Figs. 2a and 2b, respectively. It is observed that variation of E_s^* with increasing ζ_1^* is non-monotonic and a local maximum appears at a certain zeta potential. This non-monotonic nature of E_s^*–ζ_1^* correlations can be elucidated as follows. In microchannel flows, the streaming current as well as the streaming potential increases with the product of the local flow velocity and the charge density, i.e. $u \cdot \rho_e$, as that shown in Eq. (9). Increases in either fluid velocity or charge density will enhance streaming current as well as streaming potential. Increase in ζ_1^* leads to an increase in charge density but a reduction in fluid velocity in the near-wall region due to the presence of an electric force against the main flow, which is the so-called electrokinetic retardation. As the zeta potential ζ_1^* increases, therefore, the electrokinetics force is enhanced and the viscous force is reduced with the decrease in near-wall fluid velocity, whereas the sum of both forces should be equal to the driving force in a fully developed flow. The resultant streaming potential depends on the competition of these two counter effects. At the small zeta potential, the change in flow velocity is small and the variation of the charge density dominates the variation in streaming potential. As the zeta potential is further increased, however, the flow velocity in the EDL reduces remarkably due to strong retardation and the value of the product $u \cdot \rho_e$ reduces and, therefore, the streaming potential drops with the increasing value of ζ_1^*.

The parameter K can be regarded as an index for effective channel height in the viewpoint of electrokinetics. A higher value of K implies a relatively large channel height and, therefore, a weaker EDL effect. With K increased from 3 to 50, the streaming potential gradient E_s^* reduces for the weakened electrokinetic effects. As a result, the non-monotonic variation becomes mild. Therefore, the turning point or the local maximum of the E_s^*–ζ_1^* curve shifts towards a relatively higher zeta potential. In isothermal flow ($B = 0$), the values of the resultant streaming potential gradient E_s^* in CFR flows are a little higher than the corresponding values in CPG flows. With the presence of temperature non-uniformity ($B = 0.1$ and $\delta_T = 1$), the values of E_s^* in CFR flows are smaller than that in CPG flows. The results shown in Fig. 2 also reveal that the electrokinetic effect reduces with increasing K and diminishes at $K = 50$.

Electric potential and velocity distributions, ψ^* and u^*, in a typical CPG flow of strong EDL effect at conditions of $Re = 0.1, K = 3, \zeta_1^* = 4, r_\varsigma = 1, B = 0.1$ and $\delta_T = 1$, are presented in Fig. 3, and the predictions of the counterpart cases of CFR are shown in Fig. 4. The predictions of the streaming potential gradient E_s^* by various models are listed in Table 2. At the condition of strong EDL effects, the constant-property model always drastically over-predicts the streaming potential gradient at both CPG and CFR flows, while the PB and PNP solutions are close to each other. Generally, the potential distributions at conditions of relatively high zeta potential ($\zeta_1^* = 4$) and low $K(K = 3)$ shown in Figs. 3a and 4a demonstrate overlapping of the EDL. In Fig. 3a, the electrical potential solutions roughly fall into two groups. As mentioned above, the PB and PNP solutions are quite close, but the LPB deviates from them noticeably. It implies that the linearization has stronger influences on the potential solutions. The deviations of the electric potential solutions shown in Fig. 3a seem not too serious. However, in CPG flows with a given pressure gradient, the electrickinetic retardation effect may affect velocity profile considerably. Comparing with the Poseuille flow, the constant-property flow results

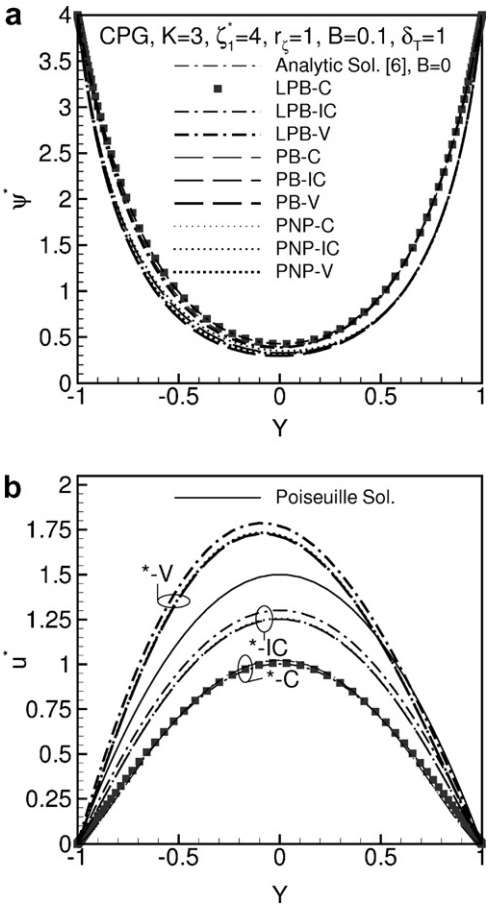

Fig. 3. (a) Electric potentials and (b) velocity profiles in CPG driving microchannel flows predicted by using various flow models.

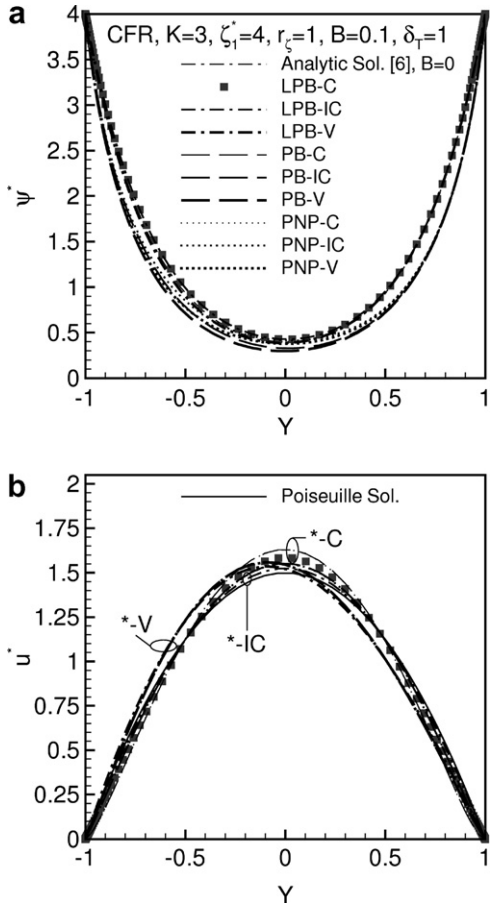

Fig. 4. (a) Electric potentials and (b) velocity profiles in CFR driving microchannel flows predicted by using various flow models.

Table 2
Predictions of streaming potential gradient E_s^* by using various models at $Re = 0.1, K = 3, \zeta_1^* = 4, r_\zeta = 1, B = 0.1, \delta_T = 1$

Model	E_s^*		
	μ, k, ε, λ, $D_\pm = C$	μ, k, $\varepsilon = C$, λ, $D_\pm = f(n_\pm)$	μ, k, $\varepsilon = f(T)$, λ, $D_\pm = f(n_\pm, T)$
A. Microchannel flows driven at constant pressure-gradient (CPG)			
LPB	24.06	9.75	9.59
PB	22.75	11.85	11.60
PNP	22.72	11.77	11.50
B. Microchannel flows driven at constant flow rate (CFR)			
LPB	37.79	11.43	8.25
PB	36.27	14.69	10.48
PNP	35.52	13.95	9.97

in Fig. 3b reveals that the flows are retarded in the presence of EDL or electrokinetic effects. The unbalanced ions in the EDL migrate towards downstream with the fluid flow leads to a generation of streaming current and streaming potential. The streaming potential generates an electric force against to the main flow and the channel flow velocity as well as flow rate are reduced. This electrokinetic retardation has been verified by a number of previous investigations on constant-property electrokinetic flows. The present results further disclose that the velocity profiles approach towards the Poiseuille solutions as the variations of $D_\pm$ and λ with ion concentration are taken into account in the computations. Considering dependence of ion concentration, the ionic diffusion $D_\pm$ and the bulk fluid conductivity λ are enhanced. Both of these two effects suppress the streaming potential and in turn alleviate the electrokinetic retardation. With further consideration of temperature-dependence of the fluid properties, the resultant velocity solutions deviate from the constant-property ones under strong retarding effects drastically. The decrease in fluid viscosity with increasing temperature compensates the reduction in flow velocity due to retardation. In the example shown in Fig. 3b, the variable-property effects not only overcome the electrokinetic retardation but also even exceed the conventional Poiseuille flow velocity. This set of predictions of microchannel flows driven at CPG demonstrates that the ion concentration- and temperature-dependence of the fluid/transport properties are significant to the electro-thermo-hydrodynamic characteristics.

In Fig. 4, the electrical potential at CFR does not change drastically. Different from the CPG cases, changes in the velocity profile at various conditions are relatively smaller. The differences between the CPG and CFR flows are due to the flow rates at different driving conditions. In CPG flows, the pressure-gradient is kept constant, but the flow rate varies case by case. As the flow retarded by the strong electrokinetic effects at this condition of low K and high ζ_1^*, the reduction in the flow rate may alter the transport phenomena dominated by the momentum transfer or forced convection. Whereas, at CFR condition, the flow rate is kept constant, the velocity distribution in the microchannel changes only slightly and the flow behaviors directly related to the velocity field have relatively smaller variation. From observations on Figs. 3 and 4, it is found that the near-wall velocities predicted by the constant-property model are lower than that by the variable-property model. This result leads to less viscous force and more electric force, which cause the over-prediction of E_s^* as that presented in Fig. 2 and Table 2.

3.4. Electric potential and streaming potential gradients

In Fig. 5a, effects of electrokinetic separation distance (K) and zeta potential (ζ_1^*) on electric potential distribution with zeta potential ratio $r_\zeta = 1$ are presented. The data in Fig. 5 are for both CPG and CFR since, with the parameters considered herein, the deviations between predictions of ψ^* in CPG and CFR flows are negligibly small. The electric potential is solved using model of PB equation with variable properties (PB-V). It is found that the results of $K = 3$,10, and 50 characterize the overlapping EDL, thick EDL, and thin EDL, respectively. The potential solutions with $K = 10$ and $\zeta_1^* = 1, 4, 8$ show that increasing zeta potential has little effect on the EDL thickness but increase electric potential in the EDL. In the case of EDL

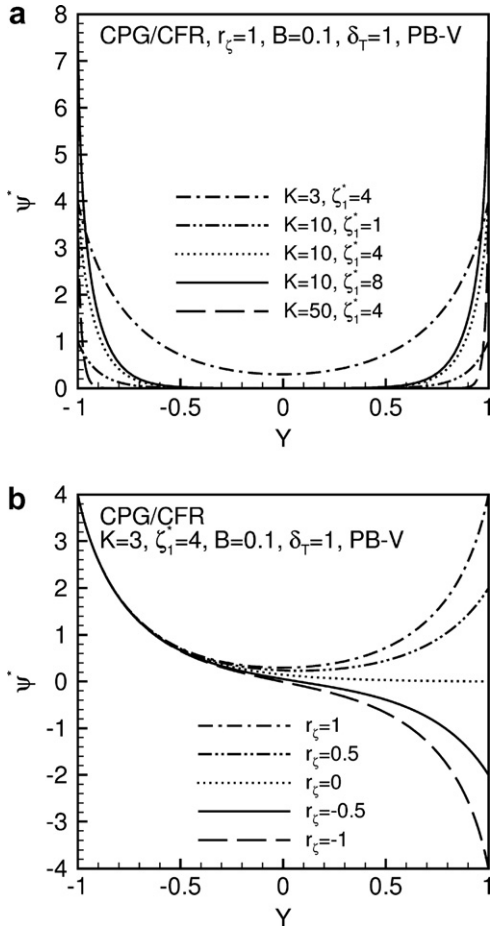

Fig. 5. Potential solutions at various conditions with effects of (a) K and ζ_1^*; (b) r_ς.

overlapped and/or $\zeta_1^* > 2$, the linear model generates noticeable deviations as shown in Fig. 2a. The potential distributions with various r_ς are plotted in Fig. 5b. With the zeta potential ratio of non-unity, the electric potential distributions between two walls are asymmetric.

Streaming potential gradients E_s^* under influences of various electric, thermal, and flow parameters are shown in Fig. 6. For both CPG and CFR flows, the value of E_s^* decreases with increasing K and it approaches zero as K up to about 50, as shown in Fig. 6a. It means that the electrokinetic effects reduce as the channel height increases. In addition, non-isothermal effects in CFR flows are more noticeable than those in CPG flows. This fact can be further demonstrated by the data in Fig. 6b, where the effects of temperature non-uniformity with $0 \leqslant B \leqslant 0.2$ are examined. At $B = 0$, the predictions of E_s^* at CPG are close to but lower than that at CFR. Qualitatively, the non-isothermal effects reduce the values of E_s^* at CPG as well as CFR conditions. As the properties presented in Appendix, increases in non-isothermal parameter B increase electric conductivity but reduce the bulk liquid viscosity. Increase in electric conductivity of the liquid results in reduction in E_s^*.In the flow driven at CPG, the retarded flow velocity can be recovered a little for lower bulk fluid viscosity in the

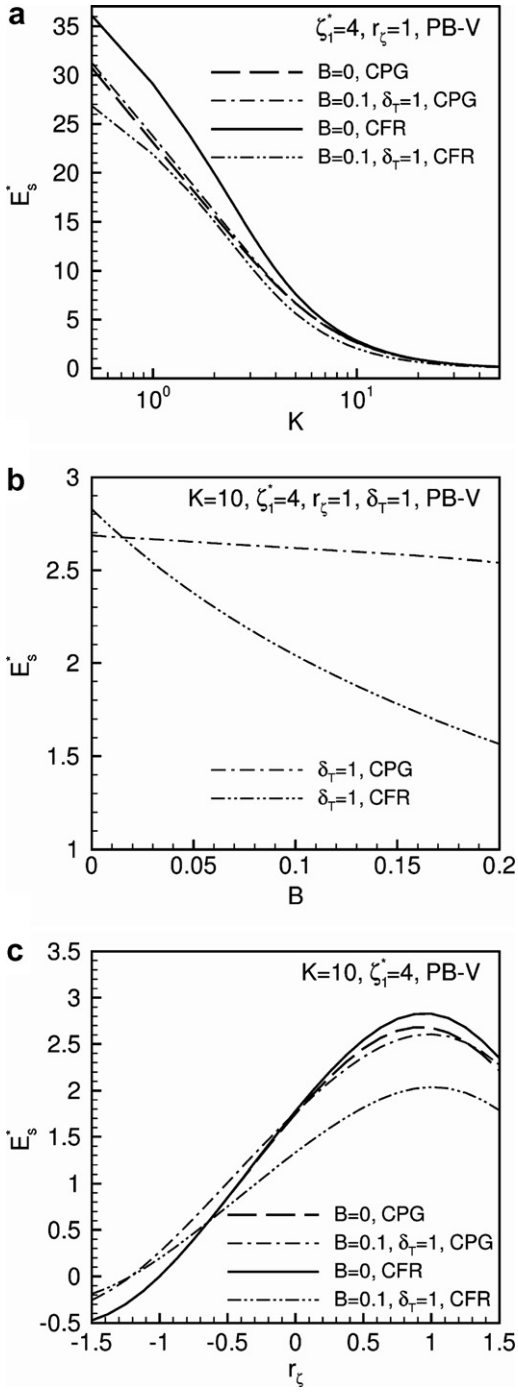

Fig. 6. Effects of (a) K; (b) B; and (c) r_ς on streaming potential gradient.

presence of non-isothermal effects. However, in CFR flows, the flow rate and thus the mean flow velocity is fixed. With B increase, electric conductivity rises up but the flow velocity by which the ion delivered downstream changes little, the value of E_s^* drops with increasing B more drastically. Consistent with the results disclosed in the previous work [6], the data in Fig. 6c show that the streaming potential in a constant-property flow ($B = 0$) is zero at $r_\varsigma = -1$ and reaches a maximal value at $r_\varsigma = 1$; while, in variable-property flows (non-zero B), this fact is modified with the

presence of temperature non-uniformity. Results in Fig. 6c also reveal that, in non-isothermal flows, the values of E_s^* at CFR are lower than the values at CPG except for $B < 0.01$ or $r_\zeta < -1.25$.

3.5. Friction factors and heat transfer rates

Fig. 7 shows the variation of the bottom-wall (wall 1) friction factor, $f_1Re(f_1 = 8\tau_{w1}/\rho U_0^2)$, with ζ_1^* in fully developed microchannel flows. It can be found that under various conditions, the friction factor f_1Re decreases as zeta potential ζ_1^* increases. For small K, the friction factors decrease more rapidly due to stronger EDL effects. The values of f_1Re may turn to negative with very strong EDL effects at small K and high ζ_1^*, which implies occurrence of the flow reversal at wall. This descending trend of the wall friction again demonstrates the electrokinetic retardation effects at high ζ_1^* and/or low K conditions. Although we have disclosed that E_s^* has a non-monotonic behavior with respect to the increasing ζ_1^*, it is worthwhile to note that there is no discrepancy between the above two facts about the f_1Re and E_s^* with the variation of ζ_1^*. Since the electric force related to electrokinetic is proportional to the product of charge density ρ_e^* and E_s^*, Eq. (11), and

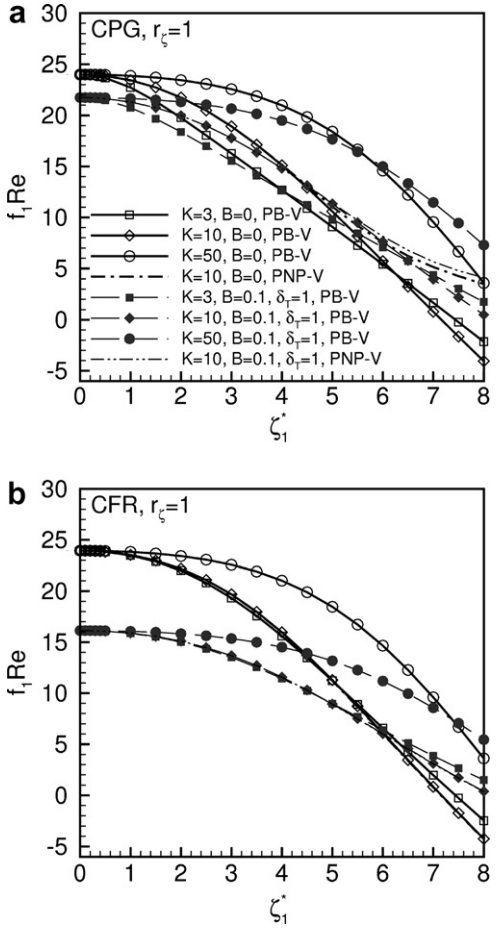

Fig. 7. Variations of friction factors with zeta potential at various effects of K and B in microchannels driven at (a) CPG; (b) CFR conditions.

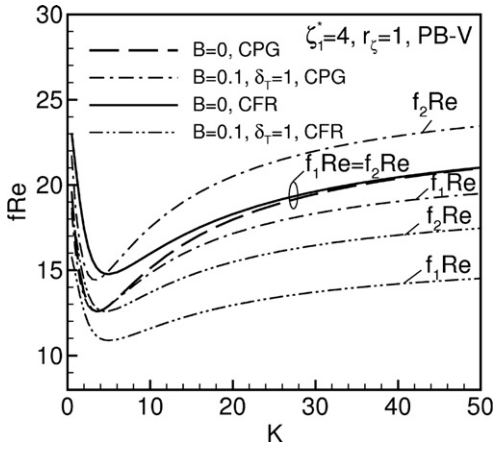

Fig. 8. PB-V predictions of friction factors in CPG and CFR flows with and without non-isothermal effects.

the monotonic increase in near-wall ρ_e^* compensates the decreases in E_s^* at high ζ_1^*. It is also observed that the non-isothermal effects reduce the value of f_1Re especially at CFR condition, and the PB solutions deviate from PNP solutions at higher ζ_1^* especially at CPG. It can be recognized that viscous force is monotonically decreased with increasing ζ_1^*. In non-isothermal flows, the decrease in f_1Re can be attributed to the reduction in viscosity at higher temperature. The difference of f_1Re between non-isothermal and isothermal flows at CFR is larger than that at CPG as that shown in Fig. 7. The reason is that the net change of driving force resulted from balance of electrokinetic retardation and variable-property effects in CFR flows is relatively smaller, therefore, lower velocity and in turn velocity gradient can be resulted in near-wall regions.

With variation in K, Fig. 8 shows the electrokinetic and non-isothermal effects on the wall friction factors f_1Re and f_2Re for $\zeta_1^* = 4$ and $r_\zeta = 1$. At isothermal condition ($B = 0$), two walls have the same friction characteristics, i.e., $f_1Re = f_2Re$, and the friction factors at CPG approaches that at CFR as K increases. While in the cases of $B = 0.1$, at both CPG and CFR conditions, the friction factors on the cold wall (f_2Re) are higher than that on the hot wall (f_1Re) due to variable properties with wall temperature asymmetry, $T_1 > T_2$. The electrokinetic effects on the hydrodynamic behaviors are related to the electric force, which is proportional to the charge density as well as the streaming potential gradient. Further, the electric potential increases with increasing charge density. In one of our previous work [6], it was disclosed that increasing K would increase electric potential but decrease streaming potential. These two counter effects render a maximum electrokinetic effect appearing at a certain value of K. The data presented in Fig. 8 demonstrate that, with increasing K, the value of fRe first decreases due to enhancement of electrokinetic retardation effect. After fRe reaches a minimum at $K \sim 4$, which corresponds to the maximum electrokinetic retardation, the fRe turns to increase with K for diminished electrokinetic effect.

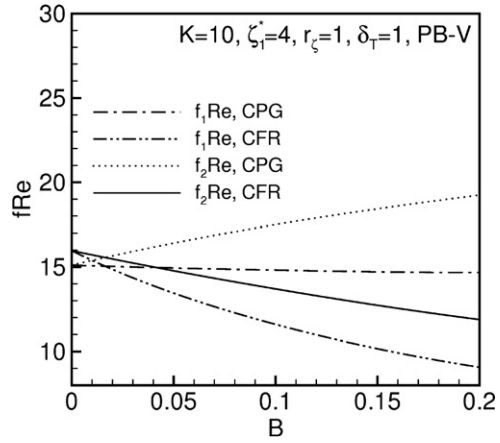

Fig. 9. Non-isothermal effects on friction factors in CPG and CFR flows.

In addition, consideration of the variable fluid and transport properties has relatively larger influences on CFR flows. To explore the detailed non-isothermal effects in the flow field, the variations of friction factor with parameter B are shown in Fig. 9. In the range of $0 \leqslant B \leqslant 0.2$, the changes of friction with the parameter B at CFR are more obvious. Consider asymmetric boundary conditions of temperature and zeta potential, results in Fig. 10 reveal quite remarkable variations of fRe with an increase in r_ζ. From the friction data presented, we can find that, at isothermal condition ($B = 0$) CFR flow has stronger driving force to overcome viscous and Coulomb forces for keeping constant flow rate, the value of fRe is higher than that in a corresponding CPG flow. With the presence of temperature gradient in the flow field ($B = 0.1$), the friction factor fRe in a CFR flow is relatively lower than that in CPG flows.

As to the heat transfer in this class of low-Reynolds-number microchannel flows, for the extremely weak forced convection, it is conduction-dominated in nature. The heat transfer rates at various electrical, thermal, hydrodynamic conditions considered in the present work deviate little

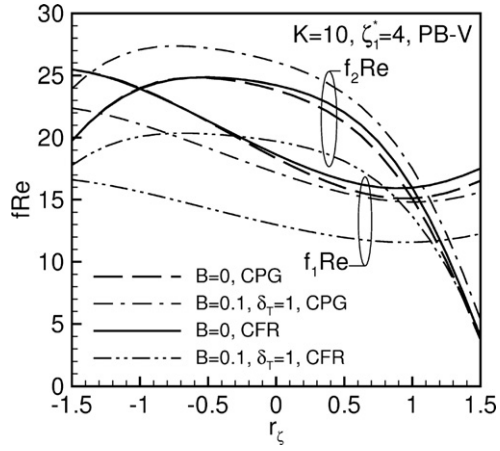

Fig. 10. Effects of zeta potential ration on friction factors in CPG and CFR flows.

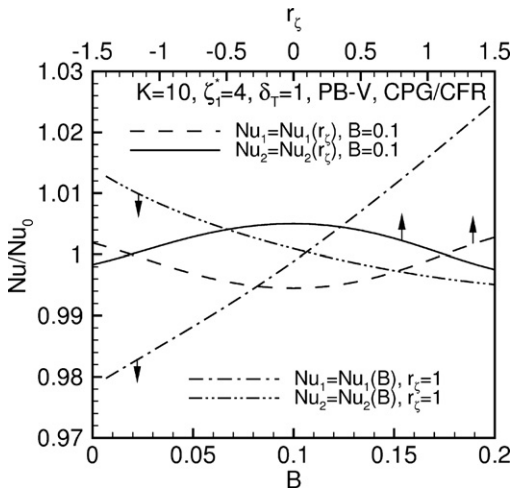

Fig. 11. Effects of temperature non-uniformity and ζ-potential ratio on Nusselt numbers in CPG and CFR flows.

from the conventional case ($Nu/Nu_0 = 1$). To demonstrate the small variation in heat transfer rate, Nusselt number normalized by that without electrokinetic effects, Nu/Nu_0, at various conditions are presented in Fig. 11. In the cases considered in the present work, the heat transfer rates with electrokinetic effects alter only a few percentages.

3.6. Flow rates and pressure-drops

In CPG flows, the pressure gradient is one of the governing parameters given a priori. The actual flow rate through the microchannel has to be evaluated by using solution of velocity distribution. In CFR flows, however, the flow rate or the mean velocity of fluid at inlet is given and the pressure loss in the microchannel is a part of solutions. Fig. 12 presents predictions of flow rate ratios, Q/Q_p, at CPG and the dimensionless pressure gradient parameter, $8(-\partial P^*/\partial X)Re$, at CFR. At CPG conditions in Fig. 12a, the flow rate is generally reduced by electrokinetic effect, but this retardation can be alleviated as K increases from 3 to a value 10 or 50. Most strikingly, taking into account variable properties with $B = 0.1$ leads to a considerable increase (about 30%) in flow rate, which implies that the flow encounters less resistance in the microchannel. The numerical and analytic solutions generated using LPB-C model agree very well but they deviate from the variable-property solutions as ζ_1^* lies up to 2. The results also demonstrate that the PB-V and PNP-V solutions agree very well, especially in the range of $\zeta_1^* < 6$. For the microchannel flows driven at CFR, the pressure drop characterized by the pressure-gradient parameter is obviously higher at a smaller value of K ($K = 3$) in Fig. 12b. Since the electrokinetic retardation is basically a resistance-increasing mechanism, the pressure drop in a CFR flow varying with the parameters K, ζ_1^*, and B has an inverse trend as the flow rate in CPG flow and can be interpreted in the same manner. The variations of Q/Q_p and $8(-\partial P^*/\partial X)Re$ with ζ_1^*

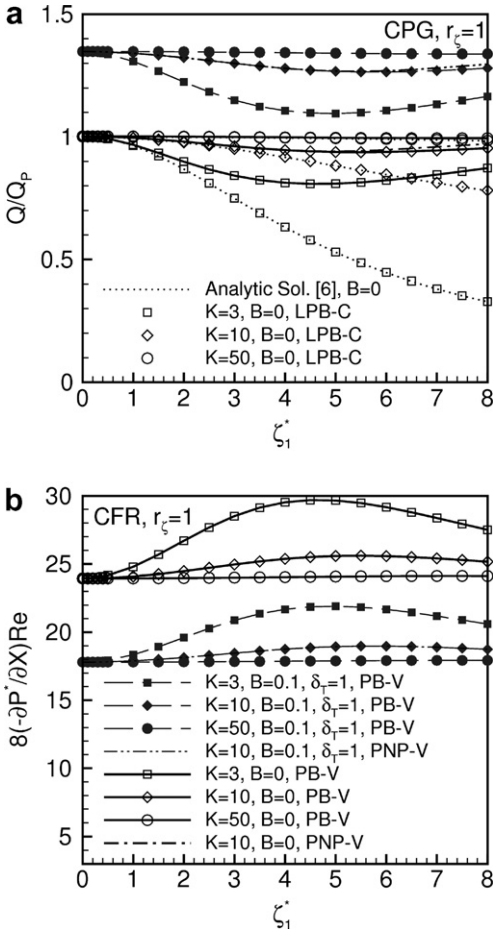

Fig. 12. Electrokinetic effects with various ζ_1^* on (a) flow rate at CPG flows, and (b) pressure drop in CFR flows predicted by constant-property and variable-property flow models.

shown in Fig. 12 have similar behavior as E_s^* shown in Fig. 2. Since the streaming potential leads to the presence of the conducting current and the electrokinetic force in the direction against the main flow. Therefore, the non-monotonic behaviors in the correlations can be addressed in the similar manner as that for E_s^* in Fig. 2.

Fig. 13 gives typical parameter-dependence of the flow rate ratio and the pressure-gradient parameter. The data in Fig. 13a show that either Q/Q_p and $8(-\partial P^*/\partial X)Re$ vary drastically with electrokinetic effects at the electrokinetic separation distance in the range of, say, $K < 20$. As shown in Fig. 13b, the flow rate in CPG or the pressure drop in CFR flows can be significantly changed by considering variable properties with the presence of non-uniform fluid temperature and ion concentration in the microchannel. However, Fig. 13c discloses that the variations in these flow characteristics are only limited for the zeta potential ratio r_ζ ranging from -1.5 to 1.5. In general, variable-property or non-isothermal effects essentially increase Q/Q_p and decrease $8(-\partial P^*/\partial X)Re$ by changing physical properties as the results shown in Figs. 13a and 13c. From Fig. 13b, it is observed that the non-isothermal effects on the flow characteristics can be further enhanced by increasing the

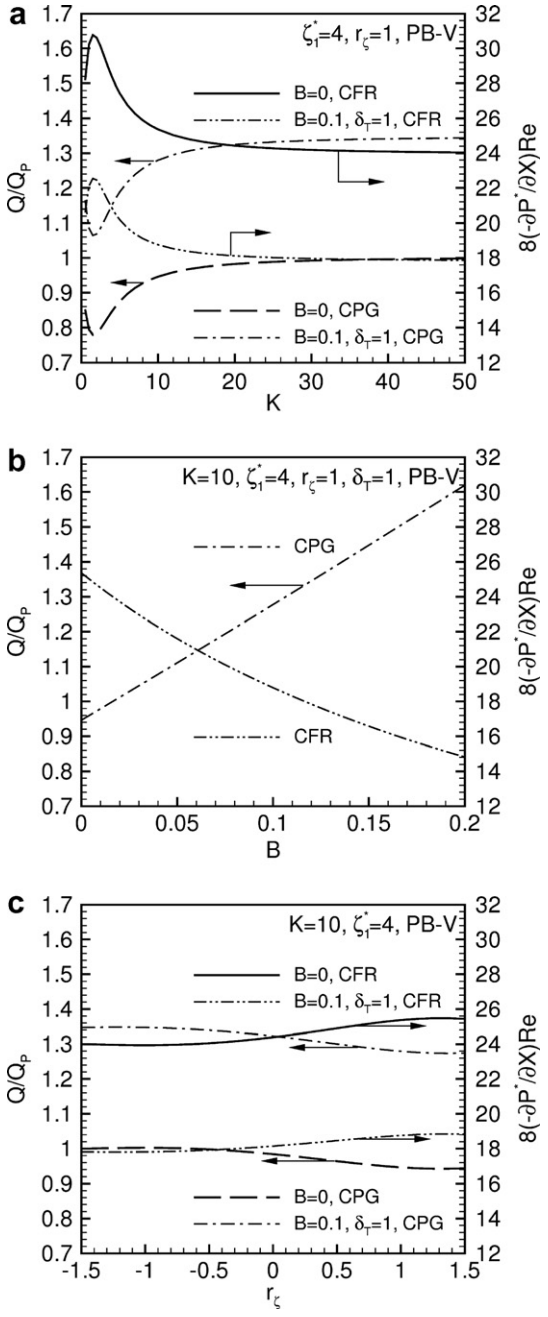

Fig. 13. Effects of (a) K; (b) B; (c) r_ζ on flow rate in CFR flows and pressure drop in CPG flows.

wall-to-fluid temperature difference characterized by the thermal parameter B.

4. Conclusions

A generalized variable-property electro-thermal flow model and the approximations of the model have been formulated and used for simulation of microchannel flows at various electrical, thermal, and hydrodynamic conditions. From the computational results and the associated analysis, the following conclusions can be drawn.

(1) For this class of low-Reynolds-number flows in microchannels, heat transfer is conduction-dominated in nature and the variations in heat transfer rate at various electrical, thermal, hydrodynamic conditions are only a few percentages. However, temperature non-uniformity significantly influences the electrical and hydrodynamic fields in microchannel flows through the ion concentration- and temperature-dependence of the fluid and transport properties. These thermal effects are relatively more pronounced in microchannel flows driven at CFR than that at CPG condition.
(2) Approximation with linearized Poisson–Boltzmann equation is appropriate for solutions at higher K ($K > 20$) and lower zeta potential ($\zeta^* < 2$). Beyond these parameter ranges, linearization is invalid for stronger electrokinetic effects and EDL overlapping. In addition, variations of physical properties with local fluid temperature and ion concentration are very influential to the flow field. The constant-property flow model with LPB potential deviates from the variable-property model remarkably.
(3) In the parameter ranges studied, the results demonstrate that the PB-V solutions agree very well with the PNP-V solutions but only little discrepancy appear at high ζ-potentials, say $\zeta_1^* > 6$. Considering the accuracy in predictions and the economics in computational time, variable-property model with PB potential is most appropriate for simulation of this class of microchannel flows without effects of strong ion convection.
(4) Different driving conditions of fluid flow, CPG or CFR, may result in different flow characteristics. The electric potential is not sensitive to the driving condition, while the streaming potential, which is a consequence of electro-thermo-hydrodynamic interaction, is of noticeable difference between the predictions at CPG and CFR conditions.
(5) Electrokinetic retardation effect enhances the flow resistance, which either reduces flow rate in CPG flows or increases the pressure drop in CFR flows. These flow characteristics can be remarkably affected by the electrokinetic separation distance (K), zeta potential level (ζ_1^*), and temperature non-uniformity (B) but relatively less influences by the zeta potential ratio (r_ζ).

Acknowledgements

The present study was supported by National Science Council of the Republic of China through Grants NSC-94-2212-E-035-012 and NSC-94-2212-E-035-020.

Appendix A. Correlations for variable properties

1. Fluid viscosity [12]

$$\mu^*(\theta) = a_5(1+B\theta)^5 + a_4(1+B\theta)^4 + a_3(1+B\theta)^3 + a_2(1+B\theta)^2 + a_1(1+B\theta) + a_0 \quad \text{(A1)}$$

$a_0 = 1.417221609884 \times 10^3$, $a_1 = -6.078267930252 \times 10^3$,
$a_2 = -1.047646763913 \times 10^4$, $a_3 = -9.057148727702 \times 10^3$,
$a_4 = 3.923681498201 \times 10^3$, $a_5 = -6.809552559312 \times 10^2$

2. Thermal conductivity [12]

$$k^*(\theta) = b_5(1+B\theta)^5 + b_4(1+B\theta)^4 + b_3(1+B\theta)^3 + b_2(1+B\theta)^2 + b_1(1+B\theta) + b \quad \text{(A2)}$$

$b_0 = 2.509960452308 \times 10^1$, $b_1 = -1.045187858138 \times 10^2$,
$b_2 = 1.747858402972 \times 10^2$, $b_3 = -1.421477914415 \times 10^2$,
$b_4 = 5.672840097532 \times 10^1$, $b_5 = -8.942042517281$

3. Permittivity [12]

$$\varepsilon^*(\theta) = c_2(1+B\theta)^2 + c_1(1+B\theta) + c_0 \quad \text{(A3)}$$

$c_0 = 3.195075035719$, $c_1 = -3.022547054553$,
$c_2 = 8.276152224113 \times 10^{-1}$

4. Electrical conductivity [22]

$$\lambda^*(\theta, n_\pm^*) = \frac{\lambda}{\lambda_0} = \frac{\lambda_+\eta_+ + \lambda_-\eta_-}{\lambda_{+0}\eta_{+0} + \lambda_{-0}\eta_{-0}} = \frac{(\lambda_{+0} + 7.45\lambda_{+0}B\theta)n_+^* + (\lambda_{-0} + 7.45\lambda_{-0}B\theta)n_-^*}{\lambda_{+0} + \lambda_{-0}} \quad \text{(A4)}$$

(K^+): $\lambda_{+0} = 73.48 \times 10^{-4}$ m^2 S/mol, (Cl^-): $\lambda_{-0} = 76.31 \times 10^{-4}$ m^2 S/mol; η_+, η_-: the number of moles of cation and anion in the electrolyte, respectively (M = kmol/m^3); λ: electrical conductivity of the electrolyte solution (S/m); λ_+, λ_-: equivalent ionic conductivity of the cations and anions, respectively. KCl is used as the electrolyte solution, and its bulk ionic concentration is chosen as 10^{-6} M. $n_+ = N_A\eta_+$, $n_- = N_A\eta_-$; N_A: Avogadro's number = 6.022×10^{23} (1/mol).

5. Ion diffusivity [23]

$$D_i = \left(\frac{RT}{F^2}\right)\left(\frac{\lambda_i}{|z_i|}\right), \quad i = +, - \ (\mathrm{m}^2/\mathrm{s}) \quad \text{(A5)}$$

$$D_\pm^* = \frac{D_\pm}{D_{\pm 0}} = \frac{T}{T_0}\frac{\lambda_\pm}{\lambda_{\pm 0}} = (1+B\theta)(1+7.45B\theta) \quad \text{(A6)}$$

D_i: diffusion coefficient of the ion in dilute aqueous solution (m^2/s).

References

[1] D. Burgreen, F.R. Nakache, Electrokinetic flow in ultrafine capillary slits, J. Phys. Chem. 68 (1964) 1084–1091.
[2] S. Levine, J.R. Marriott, N. Neale, Theory of electrokinetic flow in fine cylindrical capillaries at high ζ-potentials, J. Colloid Interface Sci. 52 (1974) 136–149.
[3] G.M. Mala, D. Li, J.D. Dale, Heat transfer and fluid flow in microchannels, Int. J. Heat Mass Transfer 40 (1997) 3079–3088.

[4] C. Yang, D. Li, J.H. Masliyah, Modeling forced liquid convection in rectangular microchannels with electrokinetic effects, Int. J. Heat Mass Transfer 41 (1998) 4229–4249.
[5] L. Ren, W. Qu, D. Li, Interfacial electrokinetic effects on liquid flow in microchannels, Int. J. Heat Mass Transfer 44 (2001) 3125–3134.
[6] C.Y. Soong, S.H. Wang, Theoretical analysis of electrokinetic flow and heat transfer in a microchannel under asymmetric boundary conditions, J. Colloid Interface Sci. 256 (2003) 202–213.
[7] C. Yang, D. Li, Electrokinetic Effects on pressure-driven liquid flow in rectangular microchannels, J. Colloid Interface Sci. 194 (1997) 95–107.
[8] P. Dutta, A. Beskok, T.C. Warburton, Numerical simulation of mixed electroosmotic/pressure driven microflows, Numer. Heat Transfer A 41 (2002) 131–148.
[9] Z. Yang, X.F. Peng, B.X. Wang, Fully developed electroosmotically and hydrodynamically induced convection between two parallel plates, Numer. Heat Transfer A 50 (2006) 905–926.
[10] T.S. Zhou, Q. Liao, Thermal effects on electro-osmotic pumping of liquids in microchannels, J. Micromech. Microeng. 12 (2002) 962–970.
[11] X.Y. Chen, K.C. Toh, J.C. Chai, C. Yang, Developing pressure-driven liquid flow in microchannels under the electrokinetic effect, Int. J. Eng. Sci. 42 (2004) 609–622.
[12] C.Y. Soong, S.H. Wang, Analysis of rotation-driven electrokinetic flow in microscale gap regions of rotating disk systems, J. Colloid Interface Sci. 269 (2003) 484–498.
[13] D. Erickson, D. Li, Analysis of alternating current electroosmotic flows in a rectangular microchannel, Langmuir 19 (2003) 5421–5430.
[14] N.T. Nguyen, Z. Wu, Micromixers – a review, J. Micromech. Microeng. 15 (2005) R1–R16.
[15] J.H. Ferziger, M. Perić, Computational Methods for Fluid Dynamics, Spring-Verlag, Berlin, Germany, 1999.
[16] J.P. Van Doormall, G.D. Raithby, Enhancements of the simple method for predicting incompressible fluid flows, Numer. Heat Transfer 7 (1984) 147–163.
[17] M.M. Rahman, T. Siikonen, An improved simple method on a collocated grid, Numer. Heat Transfer B 388 (2000) 177–201.
[18] B. Yu, H. Ozoe, W.Q. Tao, A modified pressure-correction scheme for the SIMPLER method: MSIMPLER, Numer. Heat Transfer B 39 (2001) 435–449.
[19] T. Morii, A new efficient algorithm for solving an incompressible flow on relatively fine mesh, Numer. Heat Transfer B 47 (2005) 593–610.
[20] Z.G. Qu, W.Q. Tao, Y.L. He, An improved numerical scheme for the SIMPLER method on nonorthogonal curvilinear coordinates: SIMPLERM, Numer. Heat Transfer B 51 (2007) 43–66.
[21] H.L. Stone, Iterative solution of implicit approximations of multidimensional partial equations, SIAM J. Numer. Anal. 5 (1968) 530–558.
[22] G.Y. Tang, C. Yang, J.C. Chai, H.Q. Gong, Joule heating effect on electroosmotic flow and mass species transport in a microcapillary, Int. J. Heat Mass Transfer 47 (2004) 215–227.
[23] D.R. Lide (Ed.), CRC Handbook of Chemistry and Physics, CRC Press, New York, USA, 2004, pp. 5.95–5.97.